

## DETECTION OF NEUTRAL PHOSPHORUS IN THE NEAR ULTRA-VIOLET SPECTRA OF LATE-TYPE STARS<sup>1</sup>

IAN U. ROEDERER,<sup>2</sup> HEATHER R. JACOBSON,<sup>3</sup> THANAWUTH THANATHIBODEE,<sup>3</sup> ANNA FREBEL,<sup>3</sup> ELIZABETH TOLLER<sup>3</sup>

*Accepted for publication in the Astrophysical Journal*

### ABSTRACT

We report the detection of several absorption lines of neutral phosphorus (P,  $Z = 15$ ) in archival near-ultraviolet spectra obtained with the Space Telescope Imaging Spectrograph on board the *Hubble Space Telescope*. We derive phosphorus abundances or interesting upper limits in 14 late-type stars with metallicities spanning  $-3.8 < [\text{Fe}/\text{H}] < -0.1$ . Previously, phosphorus had only been studied in Galactic stars with  $-1.0 < [\text{Fe}/\text{H}] < +0.3$ . Iron lines reveal abundance offsets between the optical and ultraviolet regions, and we discuss and apply a correction factor to account for this offset. In stars with  $[\text{Fe}/\text{H}] > -1.0$ , the  $[\text{P}/\text{Fe}]$  ratio decreases toward the solar value with increasing metallicity, in agreement with previous observational studies. In stars with  $[\text{Fe}/\text{H}] < -1.0$ ,  $\langle [\text{P}/\text{Fe}] \rangle = +0.04 \pm 0.10$ , which overlaps with the  $[\text{P}/\text{Fe}]$  ratios found in several high-redshift damped Lyman- $\alpha$  systems. This behavior hints at a primary origin in massive stars.

*Subject headings:* nuclear reactions, nucleosynthesis, abundances — stars: abundances — stars: Population I — stars: Population II

### 1. INTRODUCTION

Phosphorus (P,  $Z = 15$ ) is one of the few light elements whose nucleosynthetic origins in ancient stars remain unexamined by observations. Models by Woosley & Weaver (1995) and Kobayashi et al. (2006) predict the phosphorus yields of massive supernovae. These yields are incorporated into chemical evolution models, like those of Timmes et al. (1995) and Cescutti et al. (2012), to predict the Galactic evolution of phosphorus from the first stars until today. At present, however, no observations are capable of verifying these predictions in low-metallicity Galactic environments.

One neutron-rich isotope of phosphorus, <sup>31</sup>P, is found in solar system material. Previous derivations of the phosphorus abundance in the Sun show remarkable agreement among different studies. The earliest solar photospheric estimates by Goldberg et al. (1960) and

Lambert & Warner (1968) derived  $\log \epsilon (\text{P}) = 5.34$  and  $5.43$ , respectively, on the scale where  $\log \epsilon (\text{H}) \equiv 12.00$ . These and other estimates from the last four decades are in agreement with modern estimates by Asplund et al. (2009) and Caffau et al. (2007),  $5.41$  and  $5.46$ , respectively. These values are also in agreement with the recommended meteoritic abundance,  $5.45$  (Lodders et al. 2009).

Meléndez et al. (2009) derived phosphorus abundances in 10 solar twins, and Caffau et al. (2011) studied the evolution of phosphorus in 20 stars with  $-1.0 < [\text{Fe}/\text{H}] < +0.3$ . Phosphorus ions have been detected in the atmospheres of normal O- and B-type stars (e.g., Struve 1930; Crowther et al. 2002), the F-type star Procyon (Kato et al. 1996), chemically-peculiar A- and B-type stars on the upper main sequence or horizontal branch (e.g., Bidelman 1960; Sargent & Searle 1967; Leckrone et al. 1999; Castelli & Hubrig 2004), and hot stars that have evolved beyond the asymptotic giant branch (AGB; e.g., Vennes et al. 1996; Marcolino et al. 2007; Reiff et al. 2007). P-bearing molecules—including CP, PN, PO, HCP, C<sub>2</sub>P, and PH<sub>3</sub>—have been detected in cold, dense clouds (e.g., Turner & Bally 1987; Ziurys 1987) and the carbon- and oxygen-rich circumstellar envelopes of stars in the AGB phase of evolution (e.g., Guelin et al. 1990; Halfen et al. 2008; Milam et al. 2008; Tenenbaum & Ziurys 2008). P II has been detected in neutral gas in the interstellar medium (ISM) of the Milky Way (e.g., Morton 1975; Jenkins et al. 1986; Savage & Sembach 1996; Lehner et al. 2003). P II has been detected in the ISM of external galaxies, including the Large Magellanic Cloud (Friedman et al. 2000), M33 (Lebouteiller et al. 2006), and several more distant low-metallicity star-forming galaxies (e.g., Lebouteiller et al. 2013). P II has also been detected in several high-redshift damped Lyman- $\alpha$  systems (DLAs; Outram et al. 1999; Molaro et al. 2001; Lopez et al. 2002; Levshakov et al. 2002), and P V has been detected in the broad-absorption-line region of a quasar (Junkkarinen et al.

<sup>1</sup> Based on observations made with the NASA/ESA *Hubble Space Telescope*, obtained at the Space Telescope Science Institute, which is operated by the Association of Universities for Research in Astronomy, Inc., under NASA contract NAS 5-26555. This work is supported through program AR-13246 and is based on observations associated with programs GO-7348, GO-7433, GO-8197, GO-9048, GO-9049, GO-9455, GO-9804, GO-12268, GO-12554, and GO-12976. Portions of this work are based on data obtained from the European Southern Observatory (ESO) Science Archive Facility. These data are associated with Programs 065.L-0507(A), 067.D-0439(A), 072.B-0179(A), 074.C-0364(A), 076.B-0055(A), and 266.D-5655(A). Portions of this research have also made use of the Keck Observatory Archive (KOA), which is operated by the W.M. Keck Observatory and the NASA Exoplanet Science Institute (NExScI), under contract with the National Aeronautics and Space Administration. These data are associated with Programs H2aH (P.I. Boesgaard), H5aH (P.I. Stephens), and H47aH (P.I. Boesgaard). Other portions of this work are based on data gathered with the 6.5 meter Magellan Telescopes located at Las Campanas Observatory, Chile, and the McDonald Observatory of The University of Texas at Austin.

<sup>2</sup> Department of Astronomy, University of Michigan, 1085 S. University Ave., Ann Arbor, MI 48109, USA; iur@umich.edu

<sup>3</sup> Department of Physics & Kavli Institute for Astrophysics and Space Research, Massachusetts Institute of Technology, 77 Massachusetts Ave., Cambridge, MA 02139, USA

1997). The common theme of these extra-solar phosphorus detections is that they do not offer opportunities to confront nucleosynthesis predictions in Galactic environments with metallicity  $[\text{Fe}/\text{H}] < -1.0$ .

In contrast, extensive observations are available for the neighboring elements silicon (Si,  $Z = 14$ ) and sulfur (S,  $Z = 16$ ). Observations of Si I lines across the optical spectrum of late-type stars with  $-4.0 \leq [\text{Fe}/\text{H}] \leq +0.3$  have led to consensus regarding the cosmic origins and evolution of this element (e.g., Luck & Bond 1981; Peterson 1981; Tomkin et al. 1985; Magain 1987; Gratton & Sneden 1988; Edvardsson et al. 1993; Ryan et al. 1996; Fulbright 2000; Cayrel et al. 2004; Reddy et al. 2006; Bensby et al. 2014). Sulfur has also been systematically investigated using a few multiplets of S I in the optical and near infrared (NIR; e.g., Clegg et al. 1981; François 1987, 1988; Chen et al. 2002; Takada-Hidai et al. 2002, 2005; Reddy et al. 2003; Ecuivillon et al. 2004; Nissen et al. 2004, 2007; Ryde & Lambert 2004; Caffau et al. 2005, 2010; Nissen et al. 2007; Jönsson et al. 2011; Takeda & Takada-Hidai 2011; Spite et al. 2011; Matrozis et al. 2013). Most studies have found that both  $[\text{Si}/\text{Fe}]$  and  $[\text{S}/\text{Fe}]$  exhibit an enhanced “plateau” at low metallicity. This echos familiar trends seen in other elements produced along the  $\alpha$  chain, most notably oxygen (O,  $Z = 8$ ), magnesium (Mg,  $Z = 12$ ), and calcium (Ca,  $Z = 20$ ). Silicon and sulfur are formed primarily through  $\alpha$ -captures during hydrostatic and explosive oxygen burning, and the enhanced  $[\text{Si}/\text{Fe}]$  and  $[\text{S}/\text{Fe}]$  plateaus result from nucleosynthesis in core-collapse supernovae early in the history of the Galaxy (e.g., Matteucci & François 1989; Timmes et al. 1995; Thielemann et al. 1996; Samland 1998; Goswami & Prantzos 2000; Kobayashi et al. 2006; Tominaga et al. 2007).

In stars like the Sun, no optical lines of P I are available, and only a few weak P I multiplets are present in the NIR. These NIR lines have been known in the solar spectrum for a long time (Moore et al. 1934). Only the studies of Kato et al. (1996), Meléndez et al. (2009), and Caffau et al. (2011) have derived phosphorus abundances in stars useful for examining the nucleosynthetic fossil record. The NIR lines are too weak to detect in late-type stars with  $[\text{Fe}/\text{H}] < -1.0$ . Here we show that this observational limitation can be overcome through the use of near ultra-violet (NUV) spectroscopy of late-type stars. We examine P I absorption lines present in the near NUV spectra of late-type stars in the solar neighborhood spanning  $-3.8 < [\text{Fe}/\text{H}] < -0.1$ . Our results extend the metallicity range of stars with phosphorus abundances by nearly 3 dex.

We use standard definitions of elemental abundances and ratios. For element X, the logarithmic abundance is defined as the number of atoms of element X per  $10^{12}$  hydrogen atoms,  $\log \epsilon(X) \equiv \log_{10}(N_X/N_H) + 12.0$ . For elements X and Y, the logarithmic abundance ratio relative to the solar ratio of X and Y is defined as  $[X/Y] \equiv \log_{10}(N_X/N_Y) - \log_{10}(N_X/N_Y)_\odot$ . Abundances or ratios denoted with the ionization state indicate the total elemental abundance as derived from that particular ionization state. We adopt the Asplund et al. (2009) photospheric abundances for all elements studied.

## 2. OBSERVATIONAL DATA

We obtained observations covering the NUV spectral range from the Barbara A. Mikulski Archive for Space Telescopes (MAST). These observations were taken using the medium- or high-resolution echelle gratings in the Space Telescope Imaging Spectrograph (STIS; Kimble et al. 1998; Woodgate et al. 1998) on board the *Hubble Space Telescope* (HST). Spectra downloaded from the MAST have been reduced by the *calstis* pipeline and combined by Ayres (2010). Spectra obtained previously by our own observing programs were reduced by the *calstis* pipeline and processed as described in Roederer et al. (2012, 2014c) and Placco et al. (2014).

Some stars were discarded from our analysis because their spectra had low signal-to-noise (S/N) ratios. Cooler or more metal-rich stars were discarded because we could not reliably identify the continuum. Table 1 presents a list of the datasets and observational characteristics for the 14 stars retained for our study. Figure 1 illustrates the STIS spectra of 13 of these stars for a region surrounding the P I 2135.46 and 2136.18 Å lines. No spectrum covering these lines exists for BD+44 493, so this star is not shown in Figure 1.

We supplement these NUV spectra with optical spectra taken with ground-based telescopes and found in online archives. Table 2 provides details about these optical spectra. These data were taken using the High Accuracy Radial velocity Planet Searcher (HARPS; Mayor et al. 2003) on the ESO 3.6 m Telescope at La Silla, the Ultraviolet and Visual Echelle Spectrograph (UVES; Dekker et al. 2000) on the 8.2 m Very Large Telescope (VLT UT2, Kueyen) at Cerro Paranal, or the High Resolution Echelle Spectrometer (HIRES; Vogt et al. 1994) on the 10 m Keck I Telescope at Mauna Kea. We obtained pipeline-reduced individual exposures from the archives, normalized the continua, and shifted each exposure to laboratory-zero velocity.

Some stars were not present in these archives at the time of our query, and we have collected new optical data instead. Some observations were made using the Magellan Inamori Kyocera Echelle (MIKE) spectrograph (Bernstein et al. 2003) on the 6.5 m Landon Clay Telescope (Magellan II) at Las Campanas. These data were obtained and reduced using procedures described in detail in Roederer et al. (2014b). Other observations were obtained using the Robert G. Tull Coudé Spectrograph (Tull et al. 1995) on the 2.7 m Harlan J. Smith Telescope at McDonald Observatory. These data were reduced and combined using the REDUCE software package (Piskunov & Valenti 2002) and standard IRAF procedures. Characteristics of these observations are also given in Table 2.

## 3. STELLAR PARAMETERS

Although most stars in this sample have stellar parameters available in the literature, we carry out a homogeneous analysis based on archival optical spectra. We determine stellar parameters using a classical spectroscopic analysis starting with the measurement of equivalent widths,  $W_\lambda$ . These measurements are presented in Table 3. We use the ATLAS9 model atmosphere grid (Castelli & Kurucz 2003) and a recent version of MOOG (Sneden 1973) that includes the contribution of Rayleigh

TABLE 1  
CHARACTERISTICS OF ARCHIVAL NUV SPECTRA

Star	$\lambda$ (Å)	$R$ $\equiv \lambda/\Delta\lambda$	S/N 2136 Å	Datasets	Program ID	P.I.
BD+44 493	2280–3070	30,000	60 <sup>a</sup>	QBQ603-04	GO-12554	Beers
G64-12	2010–2810	30,000	10	O6ED01-04	GO-9049	Deliyannis
HD 2454	1970–2810	30,000	80	O6E601	GO-9048	Deliyannis
HD 16220	1990–2815	30,000	90	O6E603	GO-9048	Deliyannis
HD 43318	1990–2815	30,000	90	O6E606	GO-9048	Deliyannis
HD 76932	1880–2148	110,000	75	O8P201-02	GO-9804	Duncan
HD 94028	1885–2147	110,000	35	O5CN01-03	GO-8197	Duncan
HD 107113	$\approx$ 1800–2360	30,000	100	O4AO08	GO-7433	Heap
HD 108317	$\approx$ 1900–2365	30,000	100	OBXV01-04	GO-12976	Roederer
HD 128279	$\approx$ 1900–2365	30,000	90	OBXV05-07	GO-12976	Roederer
HD 140283	1933–2310	110,000	60	O55Z01-02	GO-7348	Edvardsson
	2370–3155	110,000	...	O6LM71	GO-9455	Peterson
HD 155646	1990–2815	30,000	35	O6E609	GO-9048	Deliyannis
HD 160617	1880–2147	110,000	30	O5CN05-06, 54	GO-8197	Duncan
HD 211998	$\approx$ 1900–2147	110,000	40	O8P203-04	GO-9804	Duncan

<sup>a</sup> S/N at 2553 Å

TABLE 2  
CHARACTERISTICS OF ARCHIVAL OPTICAL SPECTRA

Star	$\lambda$ (Å)	$R$ $\equiv \lambda/\Delta\lambda$	S/N 4500 Å	S/N 6000 Å	Instrument	Program ID	P.I.
G64-12	3420-9150	38,000	160	230	MIKE	...	Frebel
HD 2454	3780-6910	115,000	93	180	HARPS	074.C-0364(A)	Robichon
HD 16220	4350-6860	48,000	650	630	HIRES	H5aH	Stephens <sup>a</sup>
HD 43318	3100-10426	74,000	465	370	UVES	266.D-5655(A)	
HD 76932	3100-6800 <sup>b</sup>	49,000	...	315	UVES	067.D-0439(A)	Primas
					UVES	076.B-0055(A)	Silva <sup>a</sup>
					UVES	266.D-5655(A)	
HD 94028	3650-8000	30,000	430	250	Tull	...	Roederer
HD 107113	4350-6860	48,000	250	670	HIRES	H2aH	Boesgaard
HD 108317	3340-8000	38,000	570	390	MIKE	...	Roederer
HD 128279	3340-8000	38,000	880	750	MIKE	...	Roederer
HD 140283	3360-9400	38,000	390	260	MIKE	...	Frebel
HD 155646	5650-8090	48,000	...	650	HIRES	H47aH	Boesgaard
HD 160617	3100-6800 <sup>b</sup>	51,000	...	375	UVES	065.L-0507(A)	Primas
HD 211998	3100-6800 <sup>b</sup>	74,000	...	580	UVES	266.D-5655(A)	<sup>a</sup>

<sup>a</sup> Observed for inclusion in “A High-Resolution Spectroscopic Atlas of Stars across the Hertzsprung-Russell Diagram”.

<sup>b</sup> Includes gaps in the spectrum

scattering from H I in the source function (Sobeck et al. 2011).

We use the line list compiled in Roederer et al. (2010b). However, we found few Fe I and Fe II lines from this list were measurable in the spectrum of HD 155646. For this star, we use the line list from Ramírez et al. (2013). We verify that these two line lists yield similar stellar parameters and element abundances in the analysis of other metal-rich stars, and no systematic errors are introduced.

The derived model parameters are listed in Table 4. Effective temperatures ( $T_{\text{eff}}$ ) and microturbulent velocities ( $v_t$ ) are determined by minimizing trends of Fe I lines with excitation potential (E.P.) and reduced equivalent width [ $\log(W_\lambda/\lambda)$ ]. Surface gravities ( $\log g$ ) are determined by forcing the mean iron abundances derived from Fe I and Fe II lines to agree. Once excitation and ionization balance are achieved, we apply the empirical temperature calibration described in Frebel et al. (2013). Stars with  $[\text{Fe}/\text{H}] > -2.5$  fall outside the metallicity range over which this calibration was tested. We note, however, that studies of stars more metal-rich than

TABLE 3  
LINE LIST AND EQUIVALENT WIDTHS

Species	$\lambda$ (Å)	E.P. (eV)	$\log gf$	$W_\lambda$		...
				G64-12	HD 2454	
Na I	5682.63	2.10	-0.71	...	57.8	...
Na I	5688.20	2.10	-0.45	...	85.0	...
Na I	5889.95	0.00	+0.11	35.8	303.7	...
Na I	5895.92	0.00	-0.19	19.9	257.6	...
⋮	⋮	⋮	⋮	⋮	⋮	⋮

NOTE. — All  $W_\lambda$  are given in units of mÅ. The complete version of Table 3 can be found in the online edition of the journal. Only an abbreviated version is shown here to illustrate its form and content.

this have found similar discrepancies between photometric and spectroscopic  $T_{\text{eff}}$  values (e.g., Johnson 2002), indicating that a calibration such as this is appropriate. Furthermore, at the relatively warm temperatures of these stars ( $> 5200$  K), the correction is small and comparable to the uncertainty ( $< 150$  K). We have three stars in common with Nissen et al. (2007) and two in common with Asplund et al. (2006), who derived  $T_{\text{eff}}$  by

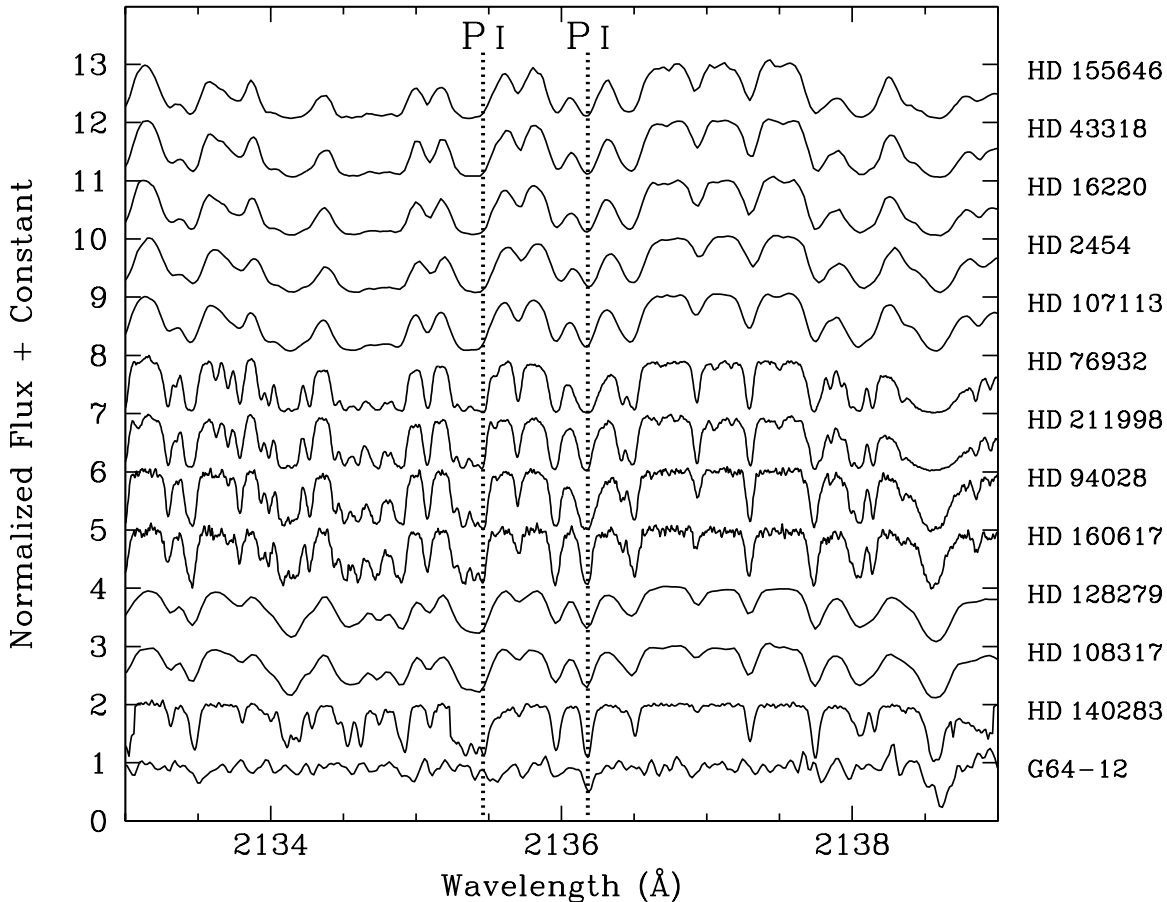


FIG. 1.— Spectral region surrounding the P I 2135.46 and 2136.18 Å lines. The STIS spectra have been shifted vertically by adding a constant to the normalized flux values. The stars are ordered by decreasing metallicity from top to bottom. The relatively clean region of continuum from 2136.6–2136.8 Å, which we use to match our observed and synthetic spectra (see Section 6), is apparent.

TABLE 4  
STELLAR PARAMETERS AND METALLICITIES

Star	$T_{\text{eff}}$ (K)	$\log g$ [cgs]	$v_t$ (km s $^{-1}$ )	[Fe/H] (dex)
BD+44 493 <sup>a</sup>	5430	3.40	1.30	-3.83
G64-12	6445	4.35	1.38	-3.28
HD 2454	6547	3.90	2.00	-0.42
HD 16220	6232	3.80	1.70	-0.31
HD 43318	6182	3.60	1.45	-0.24
HD 76932	5870	3.80	1.15	-0.92
HD 94028	5880	4.00	1.17	-1.61
HD 107113	6410	3.65	1.65	-0.59
HD 108317	5170	2.35	1.60	-2.44
HD 128279	5175	2.60	1.50	-2.37
HD 140283	5665	3.25	1.45	-2.65
HD 155646	6295	3.75	1.80	-0.17
HD 160617	5935	3.45	1.50	-1.93
HD 211998	5320	3.30	1.20	-1.50

<sup>a</sup> Parameters adopted from Ito et al. (2013)

fitting the wings of the H $\beta$  and H $\alpha$  lines, respectively. The mean differences ( $-95 \pm 57$  K and  $-72$  K, respectively) are comparable to the systematic zeropoint uncertainties of these different methods, suggesting that our results are not wildly in error.

Roederer et al. (2014b) derived stellar parameters and abundances for a large sample of metal-poor stars. That study derived  $T_{\text{eff}}$  and  $v_t$  by requiring no correlation be-

tween derived Fe I abundances and E.P. and  $\log(W_\lambda/\lambda)$ , as we have done. That study found typical statistical uncertainties of  $\approx 50$  K in  $T_{\text{eff}}$  and  $\approx 0.1$  km s $^{-1}$  in  $v_t$  for stars in similar evolutionary states to those in our sample. The uncertainties in  $T_{\text{eff}}$  and  $v_t$  when eliminating correlations with E.P. and  $\log(W_\lambda/\lambda)$  are similar in our work here. We adopt these values as the statistical uncertainties in  $T_{\text{eff}}$  and  $v_t$ . The dispersion among Fe I and Fe II lines suggests that  $\approx 0.3$  dex is a fair estimate of the statistical uncertainty in  $\log g$ . We assume that the systematic uncertainty in  $T_{\text{eff}}$  could be as large as the correction applied to convert the spectroscopic  $T_{\text{eff}}$  to the photometric ( $V - K$ ) scale (Equation 1 and Figure 2 of Frebel et al. 2013). Roederer et al. made comparisons for the derived model atmosphere parameters for large numbers of stars (see Table 9 there). The dispersions in  $\log g$  and  $v_t$  values were found to be  $\approx 0.35$  dex and  $\approx 0.4$  km s $^{-1}$  for stars in class “SG,” which have similar evolutionary states to the stars in our sample. We adopt these values as the systematic uncertainties in  $\log g$  and  $v_t$ .

We have not rederived stellar parameters or abundances for BD+44 493, and it is not listed in Table 2. This star has been studied extensively by Ito et al. (2009, 2013), Placco et al. (2014), and Roederer et al. (2014a). We do not detect P I in this star, so we simply adopt the Ito et al. (2013) model parameters and abundances.

We apply the same +0.23 dex offset to the phosphorus upper limit to correct for differences in the optical and NUV abundance scales (see Section 6.1).

#### 4. NEUTRAL PHOSPHORUS LINES DETECTABLE IN THE NUV

The high first-ionization potential of phosphorus (10.49 eV) ensures that neutral phosphorus is the dominant ionization state in the atmospheres of late-type stars. Several NUV P I lines are listed in the Atomic Spectral Database (ASD) hosted by the National Institute of Standards and Technology (NIST; Kramida et al. 2013). Among the stars in our sample, HD 140283 has the most extensive spectral coverage at  $R \sim 110,000$  and high S/N. We use this star to identify which P I lines might be reliable abundance indicators.

The P I 2135.465 Å line is clearly detected in the HD 140283 spectrum. It is blended with a Cr II line at 2135.42 Å. This line is marginally useful as an abundance indicator in HD 140283. It is illustrated in Figure 2, which compares the observed spectrum of HD 140283 with our synthetic spectra. The abundances derived from this line and all others in HD 140283 are presented in Table 5.

The P I 2136.182 Å line is approaching saturation in HD 140283. We see no evidence of line asymmetries or hints of absorption by other species in the observed line profile of HD 140283. Saturated lines are less sensitive to the abundance, but otherwise this line appears to be a reliable abundance indicator. Figure 2 illustrates this line in HD 140283.

The P I 2149.145 Å line is detected but blended with an Fe I line at 2149.18 Å. This composite feature is saturated in HD 140283 and is not useful as a phosphorus abundance indicator. This line is shown in Figure 2, but the synthetic spectrum that has been “fit” to the observed one has not been used to derive an abundance.

The P I 2152.940 Å line is located in the wing of a much stronger Fe I line at 2153.01 Å. It can be used as an abundance indicator in HD 140283, as illustrated in Figure 2.

The P I 2154.080 and 2154.121 Å transitions blend together to form one line, although the absorption is dominated by the 2154.080 Å line. They are blended with an Fe I line at 2154.13 Å of comparable strength. NIST reports a “C” accuracy (25%) for the transition probability of this Fe I line. We adjust its  $\log gf$  value in our synthesis (to  $-2.57$ ) to derive an approximate phosphorus abundance in HD 140283. Figure 2 shows our best attempt to fit this blended feature in HD 140283.

The P I 2533.976 Å line is clean, unsaturated, and easily detected in HD 140283. An unidentified absorption feature is present at 2533.89 Å. We model this feature (and all other unidentified absorption lines) as an Fe I line with an E.P. of 1.5 eV and  $\log gf$  value constrained by the observed line profile. A weak Mg I absorption feature may be present at 2534.07 Å. The P I 2533.976 Å line appears to be a reliable abundance indicator in HD 140283, as shown in Figure 2. Tests conducted using  $R \sim 30,000$  spectra of HD 108317 and HD 122563 (obtained in program GO-12268) indicate, unfortunately, that the P I 2533.976 Å line is too blended to serve as a reliable abundance indicator in lower-resolution data.

Both HD 108317 and HD 122563 have  $[\text{Fe}/\text{H}] < -2.4$ , so the P I 2533.976 Å line will not be a reliable abundance indicator in higher-metallicity stars, either.

The P I 2535.603 Å line cannot be discerned amid the absorption from a much stronger Fe I line at 2535.61 Å. Our synthesis suggests that this line would be detectable in the absence of the Fe I line. We cannot use this P I line as an abundance indicator, and it is not illustrated in Figure 2.

The P I 2553.262 Å line is detected but blended with several features of comparable strength. An unidentified feature at 2553.18 Å and a Co I feature at 2553.34 Å can be fit to match the observed line profile. Our synthesis also suggests that absorption from Mg I and Mn II could be present at 2553.26 Å, and both features are coincident with the P I line. The  $\log gf$  values of these blending features are not known from laboratory measurements. A synthesis with both the Mg I and Mn II transitions removed can generally reproduce the P I line profile. Since the Mg I and Mn II transitions could account for an unknown fraction of the absorption at this wavelength, we derive only an upper limit on the phosphorus abundance. This upper limit is larger than the phosphorus abundances derived from other, more secure, abundance indicators. Figure 2 illustrates this fit, which is computed assuming that neither Mg I nor Mn II contribute to the absorption.

Absorption is detected at the P I 2554.915 Å line. A neighboring line of Fe II at 2554.94 Å has comparable strength, and it blends with the P I line. NIST reports a “D” accuracy (50%) for the transition probability of this Fe II line. This P I line is marginally useful as an abundance indicator in HD 140283 and is illustrated in Figure 2.

In summary, there are six marginally useful P I abundance indicators in the NUV spectrum of HD 140283. Our final phosphorus abundance in HD 140283 is a mean of these six abundance derivations. In stars that are more metal-rich or cooler than HD 140283, or in spectra taken at lower resolution or with lower S/N levels, most of these lines are not useful as abundance indicators. The phosphorus abundances we derive for the other stars in our sample rely only on the P I 2136 Å line. No existing NUV spectrum of BD+44 493, however, covers the P I 2136 Å line. We derive an upper limit on the phosphorus abundance in BD+44 493 from the P I 2553 Å line assuming that no Mg I or Mn II contribute to the absorption.

## 5. ATOMIC DATA FOR PHOSPHORUS

### 5.1. Transition probabilities

Seven of the 10 P I transitions we examine in HD 140283 connect to levels in the  $^2P$  multiplet, and three connect to levels in the  $^2D$  multiplet. The upper and lower levels of each transition are listed in Table 5. Relatively little experimental work has been done on these P I transitions. Savage & Lawrence (1966) measured the radiative lifetime,  $\tau$ , of the upper  $^2P$  multiplet by the phase-shift method, finding  $\tau = 2.4 \pm 0.3$  ns. This agrees well with theoretical calculations by Lawrence (1967),  $\tau = 2.38$  ns. Savage & Lawrence also measured the lifetime of the  $^2D$  multiplet,  $2.9 \pm 0.4$  ns, which agrees with that measured using the beam-foil method

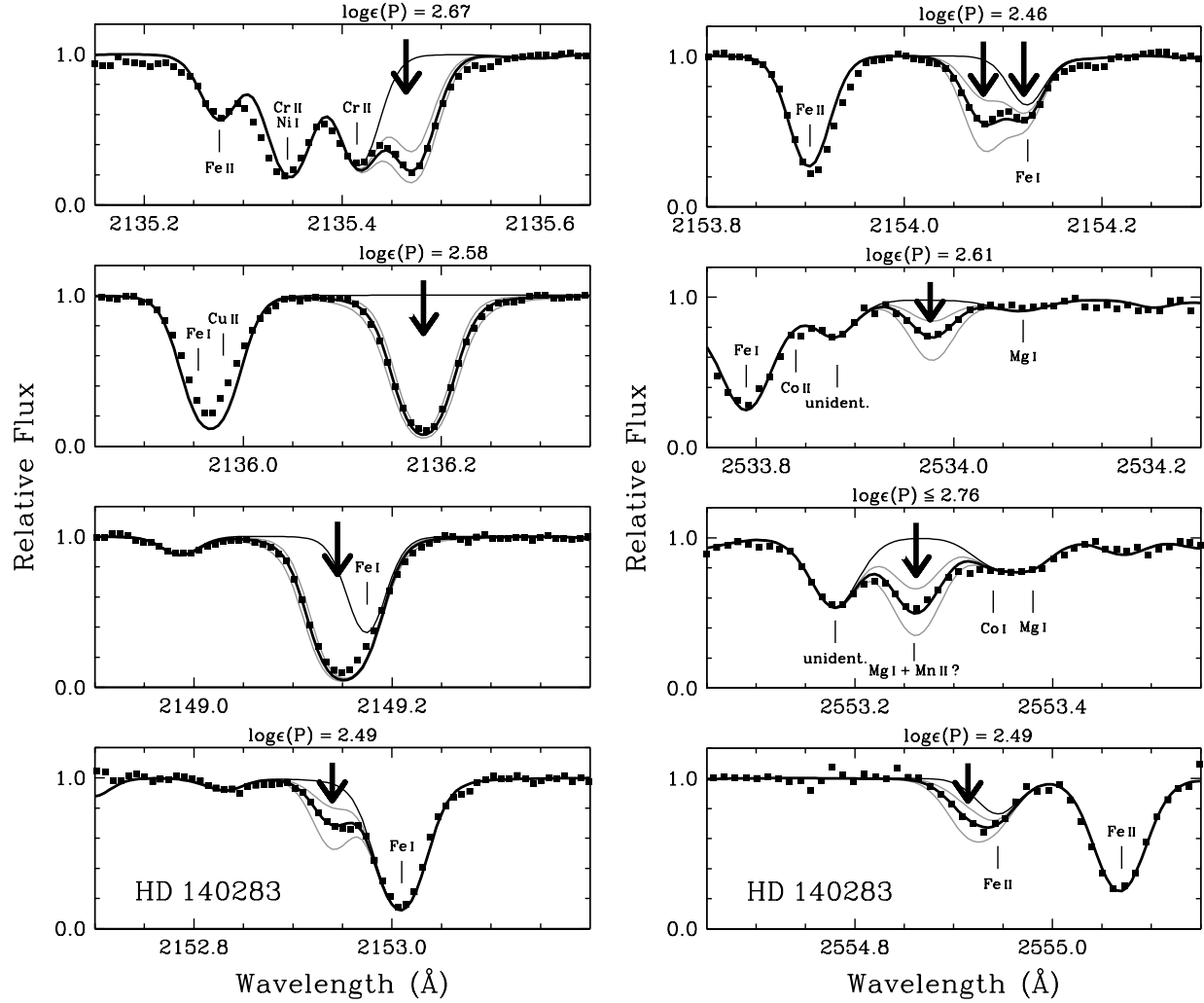


FIG. 2.— Comparison of observed (points) and synthetic (curves) spectra in HD 140283. The bold black curve marks the best fit, the thin gray curves mark variations in the best fit by  $\pm 0.3$  dex, and the thin black curve marks a synthesis with no P I absorption. Arrows mark the position of P I absorption lines. Phosphorus abundances are indicated, and the identities of blending features are marked.

TABLE 5  
ATOMIC DATA AND ABUNDANCES FOR P I LINES DETECTED IN HD 140283

Wavelength (Å)	Upper level	$E_{\text{upper}}^{\text{a}}$ ( $\text{cm}^{-1}$ )	Lower level	$E_{\text{lower}}^{\text{a}}$ ( $\text{cm}^{-1}$ )	$\log gf$	$\log \Gamma_6/N_{\text{H}}^{\text{b}}$ ( $\text{rad cm}^3 \text{ s}^{-1}$ )	$\log \epsilon$ HD 140283 <sup>c</sup>
2135.465	( <sup>3</sup> P)4s <sup>2</sup> P <sub>3/2</sub>	58174.366	3p <sup>3</sup> 2D <sub>3/2</sub> <sup>o</sup>	11361.02	-1.24	-7.42	2.67
2136.182	( <sup>3</sup> P)4s <sup>2</sup> P <sub>3/2</sub>	58174.366	3p <sup>3</sup> 2D <sub>5/2</sub> <sup>o</sup>	11376.63	-0.11	-7.42	2.58
2149.145	( <sup>3</sup> P)4s <sup>2</sup> P <sub>1/2</sub>	57876.574	3p <sup>3</sup> 2D <sub>3/2</sub> <sup>o</sup>	11361.02	-0.36	-7.42	...
2152.940	( <sup>1</sup> D)4s <sup>2</sup> D <sub>3/2</sub>	65156.242	3p <sup>3</sup> 2P <sub>1/2</sub> <sup>o</sup>	18722.71	-0.87	-7.22	2.49
2154.080	( <sup>1</sup> D)4s <sup>2</sup> D <sub>5/2</sub>	65157.126	3p <sup>3</sup> 2P <sub>3/2</sub> <sup>o</sup>	18748.01	-0.62	-7.22	2.46
2154.121	( <sup>1</sup> D)4s <sup>2</sup> D <sub>3/2</sub>	65156.242	3p <sup>3</sup> 2P <sub>3/2</sub> <sup>o</sup>	18748.01	-1.32	-7.22	<sup>d</sup>
2533.976	( <sup>3</sup> P)4s <sup>2</sup> P <sub>3/2</sub>	58174.366	3p <sup>3</sup> 2P <sub>1/2</sub> <sup>o</sup>	18722.71	-1.11	-7.42	2.61
2535.603	( <sup>3</sup> P)4s <sup>2</sup> P <sub>3/2</sub>	58174.366	3p <sup>3</sup> 2P <sub>3/2</sub> <sup>o</sup>	18748.01	-0.44	-7.42	...
2553.262	( <sup>3</sup> P)4s <sup>2</sup> P <sub>1/2</sub>	57876.574	3p <sup>3</sup> 2P <sub>1/2</sub> <sup>o</sup>	18722.71	-0.86	-7.42	$\leq 2.76$
2554.915	( <sup>3</sup> P)4s <sup>2</sup> P <sub>1/2</sub>	57876.574	3p <sup>3</sup> 2P <sub>3/2</sub> <sup>o</sup>	18748.01	-1.23	-7.42	2.49

<sup>a</sup> Svendenius (1980)

<sup>b</sup> Calculated for  $T = 10^4$  K

<sup>c</sup> Corrected for optical-NUV offset; see Section 6.1

<sup>d</sup> Line forms a blended, single feature with P I 2154.08 Å line

by Curtis et al. (1971),  $\tau = 3.6 \pm 0.4$  ns. The Lawrence theoretical calculation gives  $\tau = 2.89$  ns for this level. No experimental measures of the branching fractions (BF) are reported in the literature for any of the transitions of interest.

NIST reports  $\log gf$  values for these transitions that normalize the Lawrence (1967) BF calculations to the Savage & Lawrence (1966) lifetimes. NIST estimates a ‘‘C’’ accuracy for these values (25% or  $\approx 0.12$  dex). We infer the BFs from Lawrence’s calculations using the relation  $A_{ki} = \text{BF}/\tau$ , where  $A_{ki}$  is the transition probability. The P I 2136 Å line, which we use to derive the phosphorus abundance in all stars in our study, is a dominant branch (68%) from the  $^2P_{3/2}$  level. Its  $\log gf$  value is likely to be the least uncertain of the transitions considered. The other transitions have BFs ranging from 5% to 17%.

Lacking additional information, we simply adopt the  $\log gf$  values reported by NIST for all P I transitions in our study. These values are listed in Table 5.

### 5.2. The damping constant for the 2136 Å transition

The P I 2136 Å line shows damping wings in most stars in our sample. The strength of a spectral line with damping wings is sensitive to the number of absorbers, the oscillator strength, and the sum of the damping constants from all sources of broadening. Collisions with neutral hydrogen dominate the damping in late-type stars, so the van der Waals broadening constant,  $\Gamma_6$ , must be estimated. We adopt damping constants from the calculations of Barklem et al. (2000) and Barklem & Aspelund-Johansson (2005) when such values are available; however, these studies have not reported damping constants for any of the P I lines used in our analysis. We calculate damping constants using the same theory (Anstee & O’Mara 1995) for all 10 P I lines examined in our study. These values are presented in Table 5.

When compared with the damping constants predicted by the Unsöld (1955) approximation, the values in Table 5 are larger by factors of 1.97 (for the 2136 Å line) to 2.40. These enhancements are in line with empirical tests using Fe I lines in the Sun (e.g., Cowley et al. 1969; Simmons & Blackwell 1982; Ryan 1998). Comparisons of the Barklem et al. (2000) calculations with the Unsöld approximation suggest similar enhancements, typically factors of 1 to 2 for lines with E.P. between 1 and 2 eV.

To estimate the uncertainty in the damping constant for the P I 2136 Å line, we independently constrain the damping constant using abundances derived from other P I lines whose abundances are insensitive to the damping wings in HD 140283. If the oscillator strength and abundance are known, the damping constant of a given line can be inferred from its observed equivalent width or line profile. The mean phosphorus abundance derived from the other P I lines is lower than that derived from the 2136 Å line by 0.19 dex if no enhancement to the Unsöld (1955) approximation is adopted. Enhancement by a factor of 2 reduces the difference between the abundance derived from the 2136 Å line and the other lines to 0.14 dex, which is within the  $1\sigma$  abundance dispersion found for the other P I lines in HD 140283, 0.16 dex. For small enhancement factors, each factor of 2 enhance-

ment to the Unsöld (1955) approximation in HD 140283 reduces the derived abundance from the P I 2136 Å line by 0.05 dex. We conclude that the uncertainty in the damping constant for the P I 2136 Å line contributes less than 0.05 dex to the total abundance uncertainty.

## 6. ABUNDANCE ANALYSIS

We employ standard methods to derive abundances of phosphorus and other elements of interest. Abundances of iron, sodium, magnesium, aluminum, silicon, and calcium are derived using equivalent widths (measured from only the optical spectra), model atmospheres interpolated from the ATLAS9 grid, and the line analysis code MOOG. These results are presented in Table 6. The equivalent width, wavelength, E.P., and  $\log gf$  value of each line are presented in Table 3. All damping constants are taken from Barklem et al. (2000) and Barklem & Aspelund-Johansson (2005), when available, otherwise we resort to the Unsöld (1955) approximation for these lines.

All phosphorus abundances are derived by spectrum synthesis matching, and we use MOOG to generate the synthetic spectra. The best fits are determined by minimizing the residuals between the observed and synthetic spectra. There is a relatively clean region of continuum from 2136.6–2136.8 Å in most of our spectra. Our fits match the observed and synthetic spectra levels here. Only in the most metal-rich stars does this region begin to show weak absorption, but our synthetic spectra adequately reproduce this region. The derived phosphorus abundances are reported in Table 7.

We assess the sensitivity of the phosphorus abundances to uncertainties in the model atmosphere parameters by altering each parameter by a fixed amount. Three sets of numbers are presented in Table 8. One set corresponds to the metal-rich stars observed with moderately-high spectral resolution ( $R \sim 30,000$ ), one set corresponds to the metal-poor stars observed with moderately-high spectral resolution ( $R \sim 30,000$ ), and one set corresponds to the metal-poor stars observed with high spectral resolution ( $R \sim 110,000$ ). The stars in each group are identified in the footnotes to Table 8. The uncertainties reported in Table 8 are conservative since covariances among the model parameters are not taken into account and could reduce the abundance uncertainties by small amounts. Regardless, the abundance uncertainties are not very large ( $\lesssim 0.1$  dex), and they do not dominate the error budget.

We have also considered the effect of macroturbulence in the line profiles and derived abundances. We adopt macroturbulent velocities from Figure 3 of Valenti & Fischer (2005) and compute the macroturbulence profiles using the radial-tangential formalism presented by Gray (1992). These provide a reasonable fit to the line profiles observed in our high-resolution NUV spectra. Gaussian smoothing of our synthetic spectra also provides a reasonable fit. The derived abundances are not sensitive to these values.

### 6.1. The offset between the optical and NUV abundance scales

Previous studies of abundances derived from NUV spectra of late-type stars have uncovered evidence that

TABLE 6  
OPTICAL ABUNDANCES OF FE, NA, MG, AL, SI, AND CA

Star	[Fe/H]	<i>N</i>	[Na/Fe]	<i>N</i>	[Mg/Fe]	<i>N</i>	[Al/Fe]	<i>N</i>	[Si/Fe]	<i>N</i>	[Ca/Fe]	<i>N</i>
BD+44 493 <sup>a</sup>	-3.83 (0.19)	...	+0.30 (0.10)	...	+0.46 (0.08)	...	-0.56 (0.14)	...	+0.49 (0.14)	...	+0.31 (0.10)	...
G64-12	-3.28 (0.09)	57	-0.05 (0.13)	2	+0.37 (0.11)	3	-0.58 (0.18)	1	+0.19 (0.22)	1	+0.48 (0.14)	8
HD 2454	-0.42 (0.12)	172	+0.05 (0.15)	4	+0.07 (0.15)	3	+0.15 (0.21)	1	+0.24 (0.22)	4	+0.07 (0.16)	19
HD 16220	-0.31 (0.11)	121	+0.21 (0.15)	2	+0.12 (0.16)	1	...	0	+0.04 (0.22)	2	+0.19 (0.16)	15
HD 43318	-0.24 (0.11)	189	+0.24 (0.15)	2	-0.01 (0.13)	3	-0.23 (0.18)	2	-0.12 (0.22)	3	+0.18 (0.16)	21
HD 76932	-0.92 (0.12)	140	+0.14 (0.16)	2	+0.24 (0.15)	2	...	0	+0.05 (0.22)	3	+0.32 (0.16)	18
HD 94028	-1.61 (0.13)	234	+0.25 (0.17)	3	+0.31 (0.15)	7	-0.80 (0.22)	1	+0.27 (0.24)	2	+0.40 (0.17)	26
HD 107113	-0.59 (0.11)	135	+0.31 (0.15)	2	+0.20 (0.16)	1	...	0	+0.03 (0.22)	2	+0.22 (0.16)	20
HD 108317	-2.44 (0.11)	243	+0.62 (0.15)	2	+0.44 (0.13)	7	-1.10 (0.20)	1	+0.59 (0.23)	1	+0.44 (0.16)	26
HD 128279	-2.37 (0.12)	253	+0.26 (0.15)	4	+0.41 (0.14)	7	-0.93 (0.21)	1	+0.46 (0.22)	3	+0.42 (0.16)	26
HD 140283	-2.65 (0.08)	165	+0.24 (0.12)	2	+0.30 (0.10)	6	-0.89 (0.17)	1	+0.42 (0.21)	1	+0.33 (0.14)	20
HD 155646	-0.16 (0.07)	64	+0.20 (0.11)	2	-0.01 (0.11)	1	-0.21 (0.15)	2	+0.21 (0.19)	2	+0.10 (0.13)	8
HD 160617	-1.92 (0.08)	133	+0.53 (0.11)	4	+0.27 (0.10)	4	...	0	+0.37 (0.21)	1	+0.42 (0.14)	19
HD 211998	-1.50 (0.11)	123	-0.11 (0.15)	2	+0.30 (0.14)	2	...	0	+0.14 (0.22)	3	+0.39 (0.16)	17

<sup>a</sup> Abundances adopted from Ito et al. (2013)

TABLE 7  
PHOSPHORUS ABUNDANCES

Star	log $\epsilon$ (P)	[P/Fe]
BD+44 493	< 1.83	< +0.25
G64-12	2.28 (0.34)	+0.15 (0.26)
HD 2454	5.06 (0.27)	+0.07 (0.21)
HD 16220	4.91 (0.26)	-0.19 (0.20)
HD 43318	5.03 (0.26)	-0.14 (0.20)
HD 76932	4.93 (0.29)	+0.44 (0.20)
HD 94028	4.41 (0.29)	+0.61 (0.21)
HD 107113	5.06 (0.26)	+0.24 (0.20)
HD 108317	2.83 (0.35)	-0.14 (0.20)
HD 128279	3.08 (0.36)	+0.04 (0.22)
HD 140283	2.55 (0.30)	-0.21 (0.19)
HD 155646	5.11 (0.25)	-0.14 (0.19)
HD 160617	3.56 (0.27)	+0.07 (0.17)
HD 211998	3.78 (0.33)	-0.13 (0.21)

TABLE 8  
ABUNDANCE SENSITIVITIES TO MODEL ATMOSPHERE UNCERTAINTIES

Group	Abundance or Ratio	$\Delta T_{\text{eff}} = \pm 100$ K	$\Delta \log g = \pm 0.3$ dex	$\Delta v_t = \pm 0.2$ km s <sup>-1</sup>
Metal-rich, $R \sim 30,000^a$	[Na/Fe]	$\mp 0.02$	$\pm 0.03$	$\mp 0.03$
	[Mg/Fe]	$\mp 0.01$	$\pm 0.01$	$\mp 0.02$
	[Al/Fe]	$\mp 0.04$	$\pm 0.01$	$\mp 0.05$
	[Si/Fe]	$\mp 0.04$	$\mp 0.02$	$\mp 0.04$
	[P/Fe]	$\mp 0.01$	$\mp 0.02$	$\mp 0.02$
	[Ca/Fe]	$\mp 0.01$	$\pm 0.03$	$\mp 0.01$
	log $\epsilon$ (P)	$\pm 0.07$	$\mp 0.03$	$\mp 0.04$
	log $\epsilon$ (Fe)	$\pm 0.08$	$\mp 0.03$	$\mp 0.06$
Metal-poor, $R \sim 30,000^b$	[Na/Fe]	$\mp 0.01$	$\pm 0.04$	$\mp 0.01$
	[Mg/Fe]	$\mp 0.02$	$\pm 0.02$	$\mp 0.01$
	[Al/Fe]	$\mp 0.01$	$\pm 0.03$	$\pm 0.02$
	[Si/Fe]	$\mp 0.05$	$\mp 0.02$	$\mp 0.03$
	[P/Fe]	$\mp 0.05$	$\pm 0.02$	$\pm 0.03$
	[Ca/Fe]	$\mp 0.04$	$\pm 0.01$	$\mp 0.02$
	log $\epsilon$ (P)	$\pm 0.06$	$\mp 0.05$	$\mp 0.08$
	log $\epsilon$ (Fe)	$\pm 0.11$	$\mp 0.03$	$\mp 0.05$
Metal-poor, $R \sim 110,000^c$	[Na/Fe]	$\mp 0.02$	$\pm 0.01$	$\mp 0.02$
	[Mg/Fe]	$\mp 0.02$	$\pm 0.03$	$\mp 0.03$
	[Al/Fe]	$\pm 0.01$	$\pm 0.05$	$\mp 0.01$
	[Si/Fe]	$\mp 0.04$	$\pm 0.01$	$\mp 0.03$
	[P/Fe]	$\mp 0.03$	$\pm 0.01$	$\mp 0.01$
	[Ca/Fe]	$\mp 0.03$	$\pm 0.01$	$\mp 0.01$
	log $\epsilon$ (P)	$\pm 0.07$	$\mp 0.05$	$\mp 0.05$
	log $\epsilon$ (Fe)	$\pm 0.10$	$\mp 0.04$	$\mp 0.05$

<sup>a</sup> HD 2454, HD 16220, HD 43318, HD 107113, HD 155646

<sup>b</sup> G64-12, HD 108317, HD 128279

<sup>c</sup> HD 76932, HD 94028, HD 140283, HD 160617, HD 211998

the optical and NUV abundance scales may differ by small amounts. For example, the [Fe/H] ratio derived from Fe I lines in the optical is frequently higher than the [Fe/H] ratio derived from Fe I lines in the NUV. Furthermore, the effect is most pronounced at wavelengths in the blue near the transition from the Paschen continuum to the Balmer continuum. Roederer et al. (2010a, 2012, 2014c), Lawler et al. (2013), Wood et al. (2013, 2014), and Placco et al. (2014) have examined and discussed this issue. Presently, the origin of the discrepancy is unknown, although missing sources of continuous opacity and departures from local thermodynamic equilibrium (LTE) may each be responsible to some degree.

We have derived abundances from 5–17 Fe I and II lines in the NUV in six stars to get a sense of the magnitude of this offset in our data. These data are compared with the mean abundance derived from Fe I and II lines in the optical. Table 9 presents these results. These six stars are selected to represent the range of metallicities, stellar parameters, and data quality of our full sample. We did not derive abundances from sufficient numbers of Fe I and II lines in the NUV in the other stars to warrant inclusion in this sample.

On average, the Fe I lines in the optical yield abundances higher by  $+0.30 \pm 0.02$  dex ( $\sigma = 0.05$  dex). The Fe II lines in the optical yield abundances higher by  $+0.23 \pm 0.04$  dex ( $\sigma = 0.09$  dex). The difference between these two values,  $+0.07$  dex, suggests that non-LTE effects could be preferentially affecting low-lying levels of the minority species, Fe I, which are commonly found in the NUV. We observe an offset between the optical and NUV abundances derived from Fe II lines, too. The Fe II electronic level populations should not deviate substantially from their LTE values. This suggests that non-LTE effects are probably not the dominant source of the offset between the optical and NUV abundance scales.

Roederer et al. (2012, 2014c) also performed a detailed analysis of the Fe I and II offset for HD 108317. Figure 3 illustrates the differences in the derived abundances between that study and the present one. As expected, the agreement is good for the optical lines ( $\sigma = 0.06$  dex from 122 Fe I lines;  $\sigma = 0.07$  dex from 9 Fe II lines). The zeropoint offset ( $+0.09$  dex for Fe I;  $-0.01$  dex for Fe II) can be explained by the slightly warmer  $T_{\text{eff}}$  derived in the present study. The dispersion increases consider-



TABLE 9  
MEAN Fe I ABUNDANCES DERIVED FROM OPTICAL AND NUV LINES

Star	$\langle A(\text{Fe I}) \rangle_{\text{opt}}$	$N$	$\langle A(\text{Fe I}) \rangle_{\text{NUV}}$	$N$	$\Delta(\text{Fe I})_{\text{opt-NUV}}$	$\langle A(\text{Fe II}) \rangle_{\text{opt}}$	$N$	$\langle A(\text{Fe II}) \rangle_{\text{NUV}}$	$N$	$\Delta(\text{Fe II})_{\text{opt-NUV}}$	$\Delta(\text{Fe I-Fe II})$
HD 2454	7.08	172	6.69	16	+0.39	7.09	18	6.75	12	+0.34	+0.05
HD 16220	7.19	121	6.94	11	+0.25	7.20	13	6.88	7	+0.32	-0.07
HD 43318	7.26	189	6.99	13	+0.27	7.26	20	7.05	7	+0.21	+0.06
HD 108317	5.06	243	4.73	17	+0.33	5.07	25	4.81	13	+0.26	+0.07
HD 140283	4.85	170	4.58	5	+0.27	4.87	15	4.78	5	+0.09	+0.18
HD 155646	7.34	65	7.02	11	+0.32	7.35	5	7.15	7	+0.20	+0.12
					$\langle \Delta \rangle =$ s.e.m. =					$\langle \Delta \rangle =$ s.e.m. =	
					+0.30 0.02					+0.23 0.03	+0.07 0.03

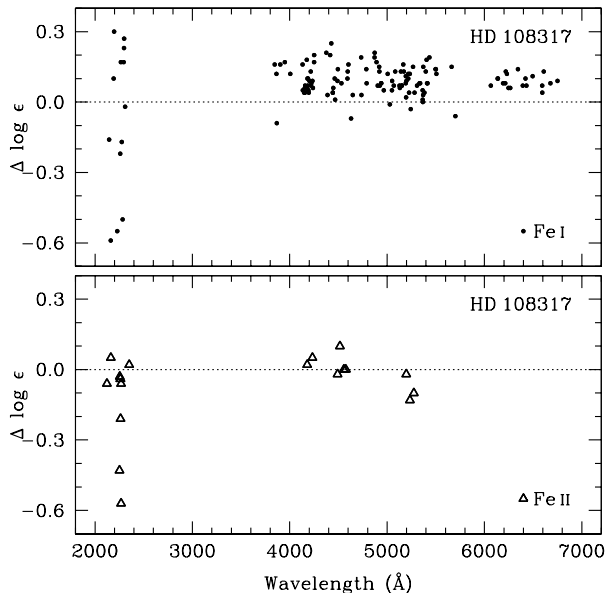


FIG. 3.— Differences in derived line-by-line abundances in HD 108317 between Roederer et al. (2012, 2014c) and our study. Differences are in the sense of our study minus Roederer et al. The top panel shows Fe I lines, and the bottom panel shows Fe II lines. The dotted line marks a difference of zero.

ably for the NUV lines near 2000 Å ( $\sigma = 0.39$  dex from 14 Fe I lines;  $\sigma = 0.22$  dex from 9 Fe II lines). Both sets of measurements show an offset in the abundances derived from lines in the NUV, but the offset derived by Roederer et al. (0.08 dex for Fe I; 0.04 dex for Fe II) is smaller than that found here (0.32 dex for Fe I; 0.18 dex for Fe II).

To minimize any potential influences from non-LTE effects on Fe I lines, we focus on the difference in Fe II, 0.14 dex (i.e., 0.18 – 0.04 dex). The analysis presented in Roederer et al. (2014c) was performed by I.U.R., while the analysis presented here was performed by H.R.J. and T.T. Both analyses used the same observed spectrum and tools for analysis. This 0.14 dex difference reflects the uncertainty that may be expected when the analysis is performed by different individuals.

We test our underlying assumption that the phosphorus and iron abundances will track each other if the continuous opacity in the NUV is altered. We artificially adjust the NUV continuous opacity in our calculations so that the abundances derived from NUV Fe I and II lines agree with the abundances derived from optical Fe I and II lines. When using the adjusted opacities, the resulting  $[\text{P}/\text{Fe}]$  ratios change by less than 0.04 dex on

average, which is less than the statistical measurement uncertainty. We conclude that our assumption is justified.

We apply a correction to our NUV abundances equal to the mean offset derived from Fe II for the six stars in Table 9, +0.23 dex. This correction is reflected in the abundances presented in Table 7. We adopt the standard error of the mean (s.e.m.) of this correction, 0.03 dex, as its statistical uncertainty. We adopt the zeropoint uncertainty in the optical-NUV abundance offset, 0.14 dex, as the systematic uncertainty in this correction.

We emphasize that this is an empirical correction designed to place abundances derived from lines in the NUV on the same scale as abundances of numerous other species derived from lines in the optical. We explicitly assume that an unknown parameter(s) is affecting the Fe II and P I lines similarly. Attempts to understand and account for the physical origin of this offset are challenging and beyond the scope of the present study. The uncertainty in this empirical correction is a substantial fraction of the total error budget, so future investigations into its origin are greatly encouraged.

## 6.2. Departures from LTE

The P I lines examined in Section 4 originate from four of the five lowest-lying levels of the neutral phosphorus atom. A simple LTE Boltzmann calculation for the conditions found in the line-forming layers of late-type stars reveals that these levels comprise  $\approx 10$ –30% of the population reservoir of neutral phosphorus. The remaining  $\approx 70$ –90% is found in the  $^4S_{3/2}$  ground level. The resonance transitions from this level are found only in the vacuum UV. The  $^2D_{5/2}^o$  level gives rise to the 2136 Å line, our primary abundance indicator, and this level alone accounts for  $\approx 5$ –16% of all neutral phosphorus in the line-forming layers. For comparison, levels in the  $^4P$  NIR Multiplet 1 employed by Caffau et al. (2011) contain  $< 0.02\%$  of the neutral phosphorus in the line-forming layers.

No non-LTE calculations exist for P I transitions under the conditions found in late-type stellar atmospheres. The relatively high percentage of neutral phosphorus found in the  $^2D_{5/2}^o$  level suggests that departures from LTE are likely to be minimal.

## 6.3. Statistical uncertainties

There are six sources of statistical uncertainty that contribute to the random errors in our phosphorus abundance derivations. Uncertainties in the  $\log gf$  values contribute 0.12 dex (Section 5.1). This term could be ne-

glected in a star-to-star differential analysis, or when only a single line is used. We include this term in the statistical uncertainty budget because abundances in two stars (BD+44 493 and HD 140283) are derived using lines other than the P I 2136 Å line. Uncertainties in the damping constant for the P I 2136 Å line contribute less than 0.05 dex (Section 5.2). The uncertainty in the mean offset between the optical and NUV abundance scales is 0.03 dex (Section 6.1). The quadrature sum of these fixed sources of random uncertainty contributes 0.14 dex toward the statistical uncertainties. We also include a term for the fitting uncertainty, which is influenced by the S/N and the line sensitivity to changes in abundance. Finally, in computing the uncertainty in [P/Fe] reported in Table 7, we add these values in quadrature with the random uncertainty in Fe I (Table 6) and the uncertainties in [P/Fe] expected from statistical uncertainties in the model atmosphere parameters (Table 8).

#### 6.4. Systematic uncertainties

We identify two sources of systematic uncertainties in the phosphorus abundance derivations. One component quantifies the impact of the model atmosphere systematic uncertainties on the phosphorus abundances (Section 6 and Table 8). The other component quantifies the zeropoint uncertainty in the NUV abundance scale relative to the optical one, 0.14 dex (Section 6.1). These values and the total statistical uncertainty (excluding the uncertainty in [P/Fe] from the model atmosphere statistical uncertainties) are used to compute the total uncertainty in  $\log \epsilon$  (P) reported in Table 7.

#### 6.5. Comparison with Caffau et al. (2011)

Unfortunately, our sample does not include any stars studied by Caffau et al. (2011), so we cannot directly assess any systematic differences. Both samples include several stars in the same metallicity range, however. If we assume that the stars in this region of metallicity overlap ( $-0.7 < [\text{Fe}/\text{H}] < -0.1$ ) sample the same underlying stellar population, we can evaluate whether any systematic differences may be present. The mean [P/Fe] ratio for the nine stars from Caffau et al. in this metallicity range is  $\langle [\text{P}/\text{Fe}] \rangle = +0.21 \pm 0.04$  dex ( $\sigma = 0.12$ ) on our solar abundance scale. In our sample, the five stars in this metallicity range have  $\langle [\text{P}/\text{Fe}] \rangle = -0.03 \pm 0.08$  dex ( $\sigma = 0.18$ ) using the abundances corrected for the optical-NUV offset. These values are in marginal agreement at the  $\approx 2\sigma$  level. If the NIR and NUV P I abundance indicators are not severely affected by departures from LTE, we assert that the +0.23 dex optical-NUV abundance offset (Section 6.1) is necessary to avoid more significant differences between our results and those of Caffau et al.

## 7. RESULTS AND DISCUSSION

Our results are illustrated in Figure 4. The left-hand panel of Figure 4 shows the odd- $Z$  elements ([Na/Fe], [Al/Fe], and [P/Fe]), and the right-hand panel of Figure 4 shows the even- $Z$  elements ([Mg/Fe], [Si/Fe], and [Ca/Fe]). Several sets of abundances derived by other studies are shown for comparison. The even- $Z$   $\alpha$ -elements exhibit the familiar pattern marked by a plateau at low metallicity and a gradual decline to the so-

lar ratios at  $[\text{Fe}/\text{H}] > -1.0$  or so. The [Na/Fe] ratios scatter about the solar value. The [Al/Fe] ratios are sub-solar at low metallicity and solar or super-solar at high metallicity. The derived sodium and aluminum abundances may be affected by departures from LTE (Gehren et al. 2004; Andrievsky et al. 2007, 2008; Lind et al. 2011). We have made no attempt to correct for this in our data, and only sodium in the Roederer et al. (2014b) comparison sample has been corrected. These corrections are negative and are large enough to explain the offset between the [Na/Fe] ratios in our study and those in the Roederer et al. study at low metallicity. Otherwise, the results for the 13 stars in our sample with phosphorus detections generally overlap with the comparison samples.

The weighted mean [P/Fe] for all 13 stars in our sample is  $+0.04 \pm 0.07$  ( $\sigma = 0.25$ ). The scatter about the mean, 0.25 dex, is comparable to the typical uncertainties in the [P/Fe] ratios, which range from 0.17 dex to 0.26 dex. A one-sided Kolmogorov-Smirnov test of the null hypothesis that these 13 stars are drawn from a normal distribution with a mean of +0.04 and standard deviation of 0.25 dex returns a  $p$ -value of 0.48. The null hypothesis cannot be excluded with any measure of confidence, and there is no compelling evidence for cosmic scatter in the [P/Fe] ratios.

Dividing the sample at  $[\text{Fe}/\text{H}] = -1.0$ , however, reveals possible differences in the high- and low-metallicity groups of stars. For the stars with  $[\text{Fe}/\text{H}] < -1.0$ , excluding BD+44 493, we derive the weighted mean ratios as follows:  $\langle [\text{P}/\text{Fe}] \rangle = +0.04 \pm 0.10$  ( $\sigma = 0.28$ ),  $\langle [\text{Na}/\text{Fe}] \rangle = +0.23 \pm 0.06$  ( $\sigma = 0.20$ ),  $\langle [\text{Mg}/\text{Fe}] \rangle = +0.34 \pm 0.02$  ( $\sigma = 0.06$ ),  $\langle [\text{Al}/\text{Fe}] \rangle = -0.85 \pm 0.09$  ( $\sigma = 0.19$ ),  $\langle [\text{Si}/\text{Fe}] \rangle = +0.35 \pm 0.06$  ( $\sigma = 0.16$ ), and  $\langle [\text{Ca}/\text{Fe}] \rangle = +0.41 \pm 0.02$  ( $\sigma = 0.05$ ). The mean [P/Fe] ratio in the low metallicity stars is about 0.2 dex lower than that predicted by one of the models by Cescutti et al. (2012),  $[\text{P}/\text{Fe}] \approx +0.2$  to  $+0.3$  dex, based on their corrected yields for massive stars. At high metallicity,  $[\text{Fe}/\text{H}] > -1.0$ , a trend of decreasing [P/Fe] with increasing [Fe/H] may be present, and is given by  $[\text{P}/\text{Fe}] = -0.86(\pm 0.32)[\text{Fe}/\text{H}] - 0.33(\pm 0.16)$ . A similar but shallower trend is also seen in the Caffau et al. (2011) data at high metallicity,  $[\text{P}/\text{Fe}] \approx -0.4[\text{Fe}/\text{H}] + 0.0$ . Type Ia supernovae are predicted to produce much smaller quantities of  $^{31}\text{P}$  (Iwamoto et al. 1999), accounting for the [P/Fe] decrease at high metallicity.

Phosphorus' behavior is consistent with that of a primary element in the stars in our sample, in the sense that it may be synthesized from hydrogen in proportions roughly equal to, e.g., the iron yield. As shown in Figure 4, this behavior is similar to that of the  $\alpha$ -elements, with a constant [P/Fe] at low metallicity. This behavior is also found in several odd- $Z$  elements not found on the  $\alpha$  chain, including potassium. Potassium has two stable isotopes,  $^{39}\text{K}$  and  $^{41}\text{K}$ , and its solar abundance is dominated by  $^{39}\text{K}$  (93%). We have not derived potassium abundances for our sample; however, an analysis of 38 subgiants with  $-3.0 \leq [\text{Fe}/\text{H}] \leq -1.0$  by Roederer et al. (2014b) finds  $\langle [\text{K}/\text{Fe}] \rangle = +0.30 \pm 0.02$  ( $\sigma = 0.15$ ). The supernova models of Woosley & Weaver (1995) predict that  $^{31}\text{P}$  and  $^{39}\text{K}$  are both primary isotopes.  $^{31}\text{P}$  is produced by neutron-capture on the products of the oxygen- and neon-burning shells in their mod-

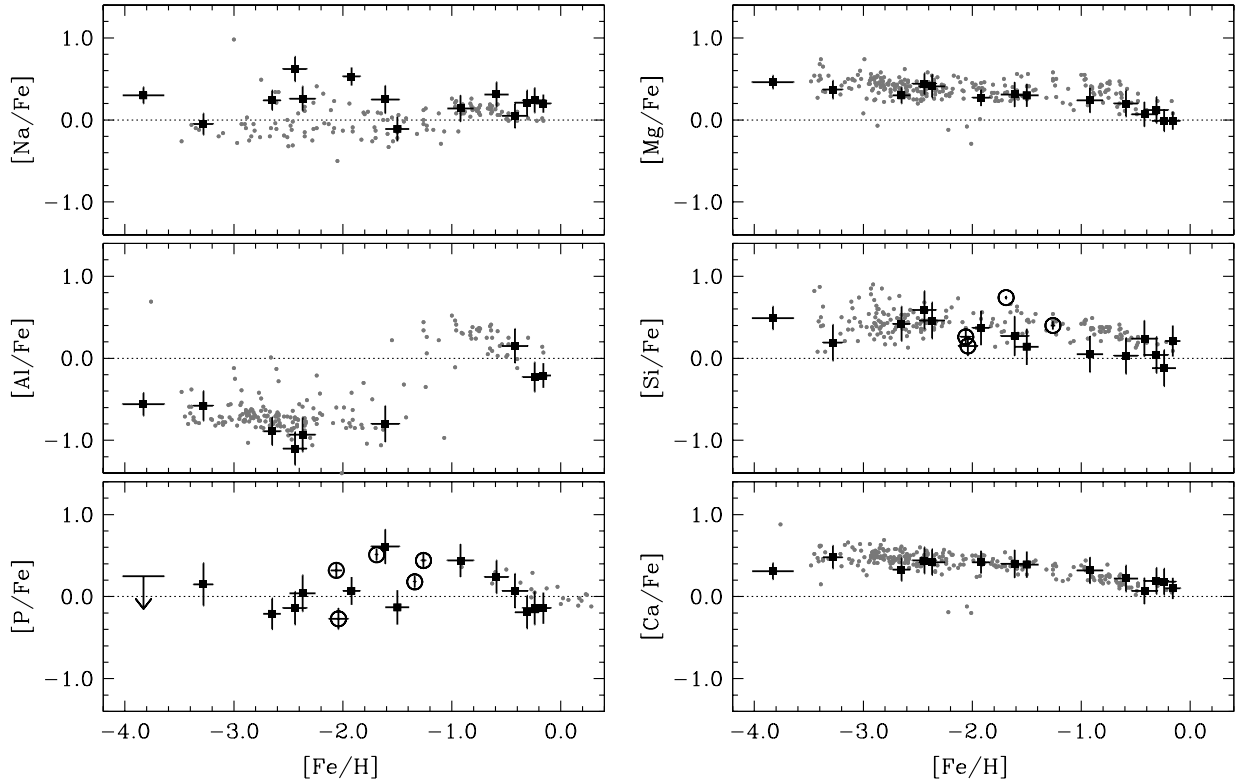


FIG. 4.— Derived abundance ratios. Stars in our sample are marked by large black symbols, and stars in the comparison samples (Fulbright 2000; Caffau et al. 2011; Roederer et al. 2014b) are marked by small gray symbols. The open circles mark detections of Si II and P II in DLA systems (Outram et al. 1999; Molaro et al. 2001; Levshakov et al. 2002; Lopez et al. 2002; R. Cooke 2014, private communication). The unpublished DLA reported by R. Cooke, J1558-0031, has abundance ratios  $[\text{Fe}/\text{H}] = -2.06$  and  $[\text{P}/\text{Fe}] = +0.32$  in a cloud at  $z_{\text{abs}} = 2.702$ ; see Cooke et al. (2014) for further details. The dotted lines mark the solar ratios.

els, and its ejection is not very sensitive to the explosion mechanism.  $^{39}\text{K}$  is also produced by oxygen burning. Our results support predictions that phosphorus, like potassium, may have a primary origin at low metallicity.

Figure 4 also shows the  $[\text{Si}/\text{Fe}]$  and  $[\text{P}/\text{Fe}]$  ratios derived from detections of Si II and P II in un- (or minimally-)depleted gas in four DLAs (Outram et al. 1999; Molaro et al. 2001; Levshakov et al. 2002; Lopez et al. 2002). These authors conclude that neither phosphorus nor iron are significantly depleted from the gas phase on dust grains in these systems. The absorbing clouds span redshifts  $2.33 \leq z \leq 3.39$ . No abundance information is available for sodium, magnesium, aluminum, or calcium in these DLAs. Our stellar abundances overlap the range of the DLA abundances, suggesting that the Galactic stars and DLAs could have been enriched by metals produced by similar nucleosynthesis channels in the early Universe.

We defer more detailed comparisons of our data with supernova yield predictions and chemical evolution models to a companion paper (Jacobson et al. 2014).

## 8. SUMMARY AND OUTLOOK

We have detected several P I absorption lines in the NUV spectra of late-type metal-poor stars. All of these detections are made using publicly-available STIS observations. We have mainly used the P I 2136.18 Å line to derive phosphorus abundances in 13 stars with  $-3.3 < [\text{Fe}/\text{H}] < -0.1$ . The P I 2553.26 Å line has

been used to derive an upper limit in one star with  $[\text{Fe}/\text{H}] = -3.8$ . Departures from LTE are likely to have a negligible impact on the derived phosphorus abundances. We also estimate the uncertainties resulting from an offset between the optical and NUV abundance scales, revealed by examination of Fe I and Fe II lines, whose cause is currently undetermined.

The derived  $[\text{P}/\text{Fe}]$  ratios compare well with previous work by Caffau et al. (2011), who used several NIR P I multiplets as abundance indicators. Our results also overlap the range of  $[\text{P}/\text{Fe}]$  ratios found in five undepleted DLA systems at high redshift. The six stars in our sample with  $[\text{Fe}/\text{H}] > -1.0$  show a decreasing trend of  $[\text{P}/\text{Fe}]$  with increasing  $[\text{Fe}/\text{H}]$ , as Caffau et al. also found. The stars with  $[\text{Fe}/\text{H}] < -1.0$  show a constant  $[\text{P}/\text{Fe}]$  ratio,  $+0.04 \pm 0.10$ , which is in marginal agreement with predictions made by the chemical evolution models of Cescutti et al. (2012).

To improve the abundance precision, the dominant sources of uncertainty must be addressed. A significant fraction of the uncertainty in the  $\log gf$  value of this line comes from the measurement uncertainty of the lifetime of its upper level (known to 13%); modern techniques routinely reach a precision of 5% (e.g., Den Hartog et al. 2011) or better (e.g., Moehring et al. 2006). Another large source of uncertainty is the offset between the optical and NUV abundance scales. A differential analysis of the same (set of) P I line(s) in stars with similar stellar parameters would minimize the uncertainty in relative abundances. Practical limitations imposed by the

stiff competition for *HST* observing time will limit future work to small numbers of bright stars, but such observations provide the only demonstrated approach to studying the nucleosynthetic origins of phosphorus in the early Galaxy.

We wish to express our appreciation to the many investigators whose observations have made this project possible. We thank R. Cooke for providing an unpublished DLA abundance that appears in Figure 4. We also thank the referee for several excellent suggestions that have improved this manuscript. Some of the data presented in this paper were obtained from the Mikulski Archive for Space Telescopes (MAST), the ESO Science Archive Facility, and the Keck Observatory Archive. STScI is operated by the Association of Universities for Research in Astronomy, Inc., under NASA contract NAS5-26555. This research has made use of NASA's Astrophysics Data

System Bibliographic Services, the arXiv pre-print server operated by Cornell University, the SIMBAD and VizieR databases hosted by the Strasbourg Astronomical Data Center, and the ASD hosted by NIST. IRAF is distributed by the National Optical Astronomy Observatories, which are operated by the Association of Universities for Research in Astronomy, Inc., under cooperative agreement with the National Science Foundation. Generous support for Program AR-13246 has been provided by NASA through a grant from the Space Telescope Science Institute, which is operated by the Association of Universities for Research in Astronomy, Incorporated, under NASA contract NAS 5-26555. The work of T. T. and E. T. was supported by the MIT UROP program. A. F. is supported by NSF CAREER grant AST-1255160.

*Facilities:* ESO:3.6m (HARPS), HST (STIS), Keck:I (HIRES), Magellan II (MIKE), Smith (Tull), VLT:Kueyen (UVES)

#### REFERENCES

- Andrievsky, S. M., Spite, M., Korotin, S. A., et al. 2007, *A&A*, 464, 1081
- Andrievsky, S. M., Spite, M., Korotin, S. A., et al. 2008, *A&A*, 481, 481
- Anstee S. D., O'Mara B. J. 1995, *MNRAS*, 276, 859
- Asplund, M., Lambert, D. L., Nissen, P. E., Primas, F., & Smith, V. V. 2006, *ApJ*, 644, 229
- Asplund, M., Grevesse, N., Sauval, A. J., & Scott, P. 2009, *ARA&A*, 47, 481
- Ayres, T. R. 2010, *ApJS*, 187, 149
- Barklem, P. S., Piskunov, N., & O'Mara, B. J. 2000, *A&AS*, 142, 467
- Barklem, P. S., & Aspelund-Johansson, J. 2005, *A&A*, 435, 373
- Bensby, T., Feltzing, S., & Oey, M. S. 2014, *A&A*, 562, A71
- Bernstein, R., Shectman, S. A., Gunnels, S. M., Mochnacki, S., & Athey, A. E. 2003, *Proc. SPIE*, 4841, 1694
- Bidelman, W. P. 1960, *PASP*, 72, 24
- Caffau, E., Bonifacio, P., Faraggiana, R., et al. 2005, *A&A*, 441, 533
- Caffau, E., Steffen, M., Sbordone, L., Ludwig, H.-G., & Bonifacio, P. 2007, *A&A*, 473, L9
- Caffau, E., Sbordone, L., Ludwig, H.-G., Bonifacio, P., & Spite, M. 2010, *Astronom. Nachr.*, 331, 725
- Caffau, E., Bonifacio, P., Faraggiana, R., & Steffen, M. 2011, *A&A*, 532, A98
- Castelli, F., & Kurucz, R. L. *Proc. IAU Symp. No 210, Modelling of Stellar Atmospheres*, N. Piskunov et al., eds. 2003, A20
- Castelli, F., & Hubrig, S. 2004, *A&A*, 425, 263
- Cayrel, R., Depagne, E., Spite, M., et al. 2004, *A&A*, 416, 1117
- Cescutti, G., Matteucci, F., Caffau, E., & François, P. 2012, *A&A*, 540, A33
- Chen, Y. Q., Nissen, P. E., Zhao, G., & Asplund, M. 2002, *A&A*, 390, 225
- Clegg, R. E. S., Tomkin, J., & Lambert, D. L. 1981, *ApJ*, 250, 262
- Cooke, R., Pettini, M., & Jorgenson, R. A. 2014, *ApJ*, submitted (arXiv:1406.7003)
- Cowley, C. R., Elste, G. H., & Allen, R. H. 1969, *ApJ*, 158, 1177
- Crowther, P. A., Hillier, D. J., Evans, C. J., et al. 2002, *ApJ*, 579, 774
- Curtis, L. J., Martinson, I., & Buchta, R. 1971, *Phys. Scr*, 3, 197
- Dekker, H., D'Odorico, S., Kaufer, A., Delabre, B., & Kotzlwski, H. 2000, *Proc. SPIE*, 4008, 534
- Den Hartog, E. A., Lawler, J. E., Sobek, J. S., Sneden, C., & Cowan, J. J. 2011, *ApJS*, 194, 35
- Ecuivillon, A., Israelian, G., Santos, N. C., et al. 2004, *A&A*, 426, 619
- Edvardsson, B., Andersen, J., Gustafsson, B., et al. 1993, *A&A*, 275, 101
- François, P. 1987, *A&A*, 176, 294
- François, P. 1988, *A&A*, 195, 226
- Frebel, A., Casey, A. R., Jacobson, H. R., & Yu, Q. 2013, *ApJ*, 769, 57
- Friedman, S. D., Howk, J. C., Andersson, B.-G., et al. 2000, *ApJ*, 538, L39
- Fulbright, J. P. 2000, *AJ*, 120, 1841
- Gehren, T., Liang, Y. C., Shi, J. R., Zhang, H. W., & Zhao, G. 2004, *A&A*, 413, 1045
- Gray, D. F. 1992, *The observation and analysis of stellar photospheres*, 2nd edition, Cambridge Univ. Press: Cambridge
- Goldberg, L., Muller, E. A., & Aller, L. H. 1960, *ApJS*, 5, 1
- Goswami, A., & Prantzos, N. 2000, *A&A*, 359, 191
- Gratton, R. G., & Sneden, C. 1988, *A&A*, 204, 193
- Guelin, M., Cernicharo, J., Paubert, G., & Turner, B. E. 1990, *A&A*, 230, L9
- Halfen, D. T., Clouthier, D. J., & Ziurys, L. M. 2008, *ApJ*, 677, L101
- Ito, H., Aoki, W., Honda, S., & Beers, T. C. 2009, *ApJ*, 698, L37
- Ito, H., Aoki, W., Beers, T. C., et al. 2013, *ApJ*, 773, 33
- Iwamoto, K., Brachwitz, F., Nomoto, K., et al. 1999, *ApJS*, 125, 439
- Jacobson, H. R., Thanathibodee, T., Frebel, A., Cescutti, G., Matteucci, F. 2014, *ApJ*, in press
- Jenkins, E. B., Savage, B. D., & Spitzer, L., Jr. 1986, *ApJ*, 301, 355
- Johnson, J. A. 2002, *ApJS*, 139, 219
- Jönsson, H., Ryde, N., Nissen, P. E., et al. 2011, *A&A*, 530, A144
- Junkkarinen, V., Beaver, E. A., Burbidge, E. M., et al. 1997, *Mass Ejection from Active Galactic Nuclei*, *Astron. Soc. Pacific Conf. Ser.* 128, ed. Arav et al., 220
- Kato, K.-I., Watanabe, Y., & Sadakane, K. 1996, *PASJ*, 48, 601
- Kimble, R. A., Woodgate, B. E., Bowers, C. W., et al. 1998, *ApJ*, 492, L83
- Kobayashi, C., Umeda, H., Nomoto, K., Tominaga, N., & Ohkubo, T. 2006, *ApJ*, 653, 1145
- Kramida, A., Ralchenko, Yu., Reader, J., et al. 2013, NIST Atomic Spectral Database (ver. 4.0–5.1) [online], available: <http://physics.nist.gov/asd>, National Institute of Standards and Technology, Gaithersburg, MD
- Lambert, D. L., & Warner, B. 1968, *MNRAS*, 138, 181
- Lawler, J. E., Guzman, A., Wood, M. P., Sneden, C., & Cowan, J. J. 2013, *ApJS*, 205, 11
- Lawrence, G. M. 1967, *ApJ*, 148, 261
- Lebouteiller, V., Kunth, D., Lequeux, J., et al. 2006, *A&A*, 459, 161
- Lebouteiller, V., Heap, S., Hubeny, I., & Kunth, D. 2013, *A&A*, 553, A16
- Leckrone, D. S., Proffitt, C. R., Wahlgren, G. M., Johansson, S. G., & Brage, T. 1999, *AJ*, 117, 1454
- Lehner, N., Jenkins, E. B., Gry, C., et al. 2003, *ApJ*, 595, 858
- Levshakov, S. A., Dessauges-Zavadsky, M., D'Odorico, S., & Molaro, P. 2002, *ApJ*, 565, 696
- Lind, K., Asplund, M., Barklem, P. S., & Belyaev, A. K. 2011, *A&A*, 528, A103

- Lodders, K., Palme, H., & Gail, H.-P. 2009, in Landolt Börnstein, New Series, Vol. VI/4B, Trümper, ed., Springer-Verlag: Berlin (arXiv:0901.1149)
- Lopez, S., Reimers, D., D'Odorico, S., & Prochaska, J. X. 2002, *A&A*, 385, 778
- Luck, R. E., & Bond, H. E. 1981, *ApJ*, 244, 919
- Magain, P. 1987, *A&A*, 179, 176
- Marcolino, W. L. F., Hillier, D. J., de Araujo, F. X., & Pereira, C. B. 2007, *ApJ*, 654, 1068
- Matrozos, E., Ryde, N., & Dupree, A. K. 2013, *A&A*, 559, A115
- Matteucci, F., & François, P. 1989, *MNRAS*, 239, 885
- Mayor, M., Pepe, F., Queloz, D., et al. 2003, *The Messenger*, 114, 20
- Meléndez, J., Asplund, M., Gustafsson, B., & Yong, D. 2009, *ApJ*, 704, L66
- Milam, S. N., Halfen, D. T., Tenenbaum, E. D., et al. 2008, *ApJ*, 684, 618
- Moehring, D. L., Blinov, B. B., Gidley, D. W., et al. 2006, *Phys. Rev. A*, 73, 023413
- Molaro, P., Levshakov, S. A., D'Odorico, S., Bonifacio, P., & Centurión, M. 2001, *ApJ*, 549, 90
- Moore, C. E., Babcock, H. D., & Kiess, C. C. 1934, *ApJ*, 80, 59
- Morton, D. C. 1975, *ApJ*, 197, 85
- Nissen, P. E., Chen, Y. Q., Asplund, M., & Pettini, M. 2004, *A&A*, 415, 993
- Nissen, P. E., Akerman, C., Asplund, M., et al. 2007, *A&A*, 469, 319
- Outram, P. J., Chaffee, F. H., & Carswell, R. F. 1999, *MNRAS*, 310, 289
- Peterson, R. C. 1981, *ApJ*, 244, 989
- Piskunov, N. E., & Valenti, J. A. 2002, *A&A*, 385, 1095
- Placco, V. M., Beers, T. C., Roederer, I. U., et al. 2014, *ApJ*, 790, 34
- Ramírez, I., Allende Prieto, C., & Lambert, D. L. 2013, *ApJ*, 764, 78
- Reddy, B. E., Tomkin, J., Lambert, D. L., & Allende Prieto, C. 2003, *MNRAS*, 340, 304
- Reddy, B. E., Lambert, D. L., & Allende Prieto, C. 2006, *MNRAS*, 367, 1329
- Reiff, E., Jahn, D., Rauch, T., et al. 2007, 15th European Workshop on White Dwarfs, *Astronom. Soc. Pacific Conf. Ser.* 372, 237
- Roederer, I. U., Sneden, C., Lawler, J. E., & Cowan, J. J. 2010a, *ApJ*, 714, L123
- Roederer, I. U., Sneden, C., Thompson, I. B., Preston, G. W., & Shtetman, S. A. 2010b, *ApJ*, 711, 573
- Roederer, I. U., Lawler, J. E., Sobeck, J. S., et al. 2012, *ApJS*, 203, 27
- Roederer, I. U., Preston, G. W., Thompson, I. B., Shtetman, S. A., & Sneden, C. 2014a, *ApJ*, 784, 158
- Roederer, I. U., Preston, G. W., Thompson, I. B., et al. 2014b, *AJ*, 147, 136
- Roederer, I. U., Schatz, H., Lawler, J. E., et al. 2014c, *ApJ*, 791, 32
- Ryan, S. G. 1998, *A&A*, 331, 1051
- Ryan, S. G., Norris, J. E., & Beers, T. C. 1996, *ApJ*, 471, 254
- Ryde, N., & Lambert, D. L. 2004, *A&A*, 415, 559
- Samland, M. 1998, *ApJ*, 496, 155
- Sargent, W. L. W., & Searle, L. 1967, *ApJ*, 150, L33
- Savage, B. D., & Lawrence, G. M. 1966, *ApJ*, 146, 940
- Savage, B. D., & Sembach, K. R. 1996, *ApJ*, 470, 893
- Simmons, G. J., & Blackwell, D. E. 1982, *A&A*, 112, 209
- Sneden, C. A. 1973, Ph.D. Thesis, University of Texas at Austin
- Sobeck, J. S., Kraft, R. P., Sneden, C., et al. 2011, *AJ*, 141, 175
- Spite, M., Caffau, E., Andrievsky, S. M., et al. 2011, *A&A*, 528, A9
- Struve, O. 1930, *ApJ*, 71, 150
- Svendenius, N. 1980, *Phys. Scr*, 22, 240
- Takada-Hidai, M., Takeda, Y., Sato, S., et al. 2002, *ApJ*, 573, 614
- Takada-Hidai, M., Saito, Y.-J., Takeda, Y., et al. 2005, *PASJ*, 57, 347
- Takeda, Y., & Takada-Hidai, M. 2011, *PASJ*, 63, 537
- Tenenbaum, E. D., & Ziurys, L. M. 2008, *ApJ*, 680, L121
- Thielemann, F.-K., Nomoto, K., & Hashimoto, M.-A. 1996, *ApJ*, 460, 408
- Timmes, F. X., Woosley, S. E., & Weaver, T. A. 1995, *ApJS*, 98, 617
- Tominaga, N., Umeda, H., & Nomoto, K. 2007, *ApJ*, 660, 516
- Tomkin, J., Lambert, D. L., & Balachandran, S. 1985, *ApJ*, 290, 289
- Tull, R. G., MacQueen, P. J., Sneden, C., & Lambert, D. L. 1995, *PASP*, 107, 251
- Turner, B. E., & Bally, J. 1987, *ApJ*, 321, L75
- Unsöld, A., *Physik der Sternatmosphären*, Springer-Verlag, Berlin, 1955, p. 332
- Valenti, J. A., & Fischer, D. A. 2005, *ApJS*, 159, 141
- Vogt, S. S., Allen, S. L., Bigelow, B. C., et al. 1994, *Proc. SPIE*, 2198, 362
- Vennes, S., Chayer, P., Hurwitz, M., & Bowyer, S. 1996, *ApJ*, 468, 898
- Wood, M. P., Lawler, J. E., Sneden, C., & Cowan, J. J. 2013, *ApJS*, 208, 27
- Wood, M. P., Lawler, J. E., Sneden, C., & Cowan, J. J. 2014, *ApJS*, 211, 20
- Woodgate, B. E., Kimble, R. A., Bowers, C. W., et al. 1998, *PASP*, 110, 1183
- Woosley, S. E., & Weaver, T. A. 1995, *ApJS*, 101, 181
- Ziurys, L. M. 1987, *ApJ*, 321, L81